Journal of Sound and Vibration (2001) **242**(4), 719–735
doi:10.1006/jsvi.2000.3340, available online at http://www.idealibrary.com on IDEAL®

THE MEASUREMENT OF STRUCTURE-BORNE SOUND ENERGY FLOW IN AN ELASTIC CYLINDRICAL SHELL

R. S. Ming, J. Pan and M. P. Norton

Department of Mechanical and Materials Engineering, The University of Western Australia, Nedlands WA 6907, *Australia. E-mail*: *rming@mech.uwa.edu.au*

(*Received* 14 *April* 2000, *and in final form* 20 *September* 2000)

Structural waves in a cylindrical shell can be decomposed into different circumferential modes. The energies carried by these modes usually need to be quantified and ranked for the purposes of noise and vibration control. In this paper, a theoretical basis is outlined for a method to measure the energy flow components of different circumferential modes through a cross-section of a circular cylindrical shell. This new method has potential to measure energy flow carried by higher order circumferential modes ($n \geqslant 3$). Experimental results obtained on a thin-walled circular cylindrical shell show that this proposed method can be used to accurately measure the total energy flow and its components.

1. INTRODUCTION

Structural vibration of a cylindrical shell exhibits a modal pattern in the circumferential direction. Each circumferential mode may have several axial wave types such as flexural, extensional and torsional waves characterized by purely real, purely imaginary or complex wavenumbers. As far as energy flow is concerned, only those with purely real wavenumbers are of interest because the energy carried by the corresponding waves propagates away from the source region. Different wave types may exchange energy as they come across the discontinuity along cylindrical shells. To illustrate the behaviour of the energy flow through a cross-section of a cylindrical shell, it is necessary to distinguish and determine all the participating energy flow components associated with different circumferential modes.

The structural intensity technique has the ability to distinguish and rank the energy flows of different wave types. Most of its application is concentrated on beams and plates [1–5]. Verheij [6, 7] has applied the farfield (two-transducer) intensity technique to measure the energy flow components in fluid-filled cylindrical shells. The technique provides a practical method to measure the energy flow in pipes at frequencies below the cut-off frequency of the $n = 2$ circumferential mode. Later, Jong and Verheij [8] proposed a method to extend the upper frequency limit to the cut-off frequency of the $n = 3$ circumferential mode. This method utilizes the symmetrical nature of the circular cylindrical shell and a group of accelerometers on the shell surface to obtain the circumferential modal amplitudes and phases. Briscoe and Pinnington [9] have presented several different techniques for the measurement of $n = 0$ axisymmetric wave energy flows in fluid-filled and empty circular cylindrical shells. Their intensity probes consists of accelerometers and PVDF sensors, or their combination.

For cylindrical shells with large diameters, the cut-off frequencies of $n = 3$ and 4 circumferential modes may be within the frequency range of interest. The work presented in

0022-460X/01/190719 + 17 $35.00/0

this paper is a natural extension of the previous method for the measurement of total energy flow and its components in a uniform circular cylindrical shell. This method uses an array of accelerometers to simultaneously measure dynamical responses at several positions around the cross-sections of interest in a cylindrical shell. Then the method of least squares [10] is used to determine the polarization angle of each circumferential model and to obtain the axial, tangential and radial acceleration components of every circumferential mode at these cross-sections. The Flugge theory [11] is applied to formulate the energy flow. A laboratory experiment was carried out to verify this proposed method and the assessment is made based on the direct measurement of input power using an impedance head and the method described in reference [8].

The work described in this paper may be significant because:

- it extends the upper limit of the frequency range for energy flow measurement in pipeline systems to above the cut-off frequency of $n = 3$ circumferential mode;
- in principle, this method allows the measurement of total energy flow, even though only part of the cross-section of the cylindrical shell is accessible.

2. ENERGY FLOW

Consider a uniform thin-walled circular cylindrical shell of thickness h and mean radius a. The midsurface of the shell is described in an (a, θ, x) cylindrical co-ordinate, as shown in Figure 1. If u, v and w represent the displacement components of the shell midsurface in the axial, tangential and radial directions, respectively, the instantaneous axial structural intensity component can be expressed as [12]

$$I_x = -\sigma_x \frac{\partial u}{\partial t} - \tau_{x\theta} \frac{\partial v}{\partial t} - \tau_{xr} \frac{\partial w}{\partial t}, \tag{1}$$

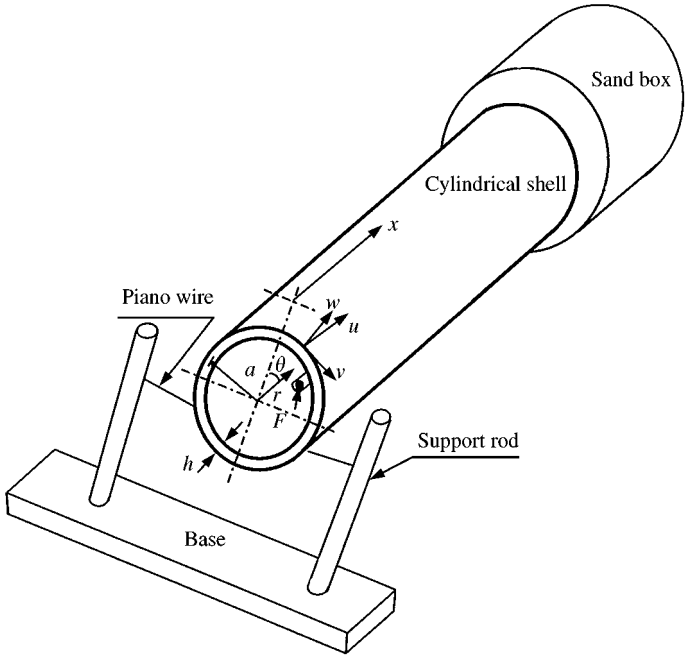

Figure 1. Schematic diagram of the experimental set-up.

where σ_x is the normal stress, and $\tau_{x\theta}$ and τ_{xr} are the shear stresses in the tangential and radial directions at the cross-section of x [11]. The time-averaged total axial structural energy flow across a cross-section is given by [11]

$$P_x = \int_0^{2\pi} \int_{-h/2}^{h/2} \langle I_x \rangle_t \left(1 + \frac{z}{a}\right) a \, \mathrm{d}z \, \mathrm{d}\theta, \tag{2}$$

where $\langle\ \rangle_t$ means the temporal average. The temporal average in the time domain has equivalent operations in the frequency domain [3]. In the frequency domain, the dependence of displacement components, u, v and w, on θ can be assumed in the following forms [11, 13]:

$$u = u_0 + \sum_{n=1}^{\infty} u_n \cos(n\theta + \theta_{n0}), \quad v = \sum_{n=1}^{\infty} v_n \sin(n\theta + \theta_{n0}),$$

$$w = w_0 + \sum_{n=1}^{\infty} w_n \cos(n\theta + \theta_{n0}), \tag{3}$$

where n is the circumferential modal number, θ_{n0} is a constant number representing the polarization angle of the nth circumferential mode, and u_n, v_n and w_n are the functions of x and radian frequency ω respectively. In general, $\theta_{n0} = n\theta_{10}$ does not hold. For a single-force excitation, however, this relation will hold. For the breathing mode $n = 0$, the tangential displacement component v_0 is usually not equal to zero in practice and needs to be considered during the measurements. The non-zero value of $v = v_0$ represents a pure torsional wave propagating along the cylindrical shell and it is uncoupled from the other two orthogonal displacement components, u_0 and w_0.

If the Flugge theory [11] is adopted, in the frequency domain the Fourier transform of equation (2) can be expressed as

$$P_x = \sum_{n=0}^{\infty} (P_{xL}^n + P_{xT}^n + P_{xB}^n), \tag{4}$$

where

$$\begin{aligned}
P_{xL}^n &= D \,\mathrm{Im}\left\{\left[B_1\left(\frac{\partial \tilde{u}_n}{\partial x} + \frac{\mu}{a}(\tilde{w}_n + n\tilde{v}_n)\right) - \frac{B_2}{a}\frac{\partial^2 \tilde{w}_n}{\partial x^2}\right]\tilde{u}_n^*\right\},\\
P_{xT}^n &= \frac{(1-\mu)D}{2}\,\mathrm{Im}\left\{\left[\left(B_1 + \frac{B_2}{a^2}\right)\frac{\partial \tilde{v}_n}{\partial x} - \frac{nB_1}{a}\tilde{u}_n + \frac{nB_2}{a^2}\frac{\partial \tilde{w}}{\partial x}\right]\tilde{v}_n^*\right\},\\
P_{xB}^n &= D \,\mathrm{Im}\left\{\begin{array}{l} B_2\left[\dfrac{\partial^3 \tilde{w}_n}{\partial x^3} - \dfrac{\mu n^2}{a^2}\dfrac{\partial \tilde{w}_n}{\partial x} - \dfrac{1}{a}\dfrac{\partial^2 \tilde{u}_n}{\partial x^2} - \dfrac{(1-\mu)n^2}{2a^3}\tilde{u}_n - \dfrac{(1+\mu)n}{2a^2}\dfrac{\partial \tilde{v}_n}{\partial x}\right]\tilde{w}_n^* \\ - B_2\left[\dfrac{\partial^2 \tilde{w}_n}{\partial x^2} - \dfrac{\mu n^2}{a^2}\tilde{w}_n - \dfrac{1}{a}\dfrac{\partial \tilde{u}_n}{\partial x} - \dfrac{\mu n}{a^2}\tilde{v}_n\right]\dfrac{\partial \tilde{w}_n^*}{\partial x}\end{array}\right\},
\end{aligned} \tag{5}$$

$$D = \frac{\varepsilon_n \pi a \omega}{2}, \quad B_1 = \frac{Eh}{1-\mu^2}, \qquad B_2 = \frac{Eh^3}{12(1-\mu^2)},$$

where μ is the Poisson ratio, $\sim$ denotes a Fourier transform, * denotes a complex conjugate and Im means the imaginary part. $\varepsilon_0 = 2$ and $\varepsilon_n = 1$ for $n > 1$. When the radius a becomes infinite, the components P_{xL}^n, P_{xT}^n and P_{xB}^n correspond to the extensional,

torsional and flexural wave energy flows in a uniform plate respectively (πa in the parameter D is equal to the plate width). Using the finite difference approximation, the first order partial derivative of displacement with respect to x can be approximated from the displacements measured at two close cross-sections [2]. However, the terms P^n_{xL} and P^n_{xB} contain the second and third partial derivatives. Therefore, in general, the estimation of energy flow in equation (4) needs to measure all the displacement components, u, v and w, at four neighbouring cross-sections.

If the cross-section (or positions) of interest is in the far field where decaying waves are insignificant and if only one single real wavenumber k_n is present for each circumferential number n in the frequency range of interest (this is usually the case at low frequencies), the second order partial derivatives of $\tilde{u}_n$ and $\tilde{w}_n$ can be rewritten as

$$\frac{\partial^2 \tilde{u}_n}{\partial x^2} = -k_n^2 \tilde{u}_n, \qquad \frac{\partial^2 \tilde{w}_n}{\partial x^2} = -k_n^2 \tilde{w}_n. \tag{6}$$

Substituting the above equation into equation (5) gives

$$P^n_{xL} = D \operatorname{Im}\left\{\left[B_1\left(\frac{\partial \tilde{u}_n}{\partial x} + \frac{n\mu}{a}\tilde{v}_n\right) + \frac{(\mu B_1 + B_2 k_n^2)}{a}\tilde{w}_n\right]\tilde{u}_n^*\right\},$$

$$P^n_{xB} = D \operatorname{Im}\left\{\begin{array}{l} B_2\left[-2\left(k_n^2 - \dfrac{\mu n^2}{a^2}\right)\dfrac{\partial \tilde{w}_n}{\partial x} + \left(\dfrac{k_n^2}{a} - \dfrac{(1-\mu)n^2}{2a^3}\right)\tilde{u}_n - \dfrac{(1+\mu)n}{2a^2}\dfrac{\partial \tilde{v}_n}{\partial x}\right]\tilde{w}_n^* \\ + B_2\left[\dfrac{1}{a}\dfrac{\partial \tilde{u}_n}{\partial x} + \dfrac{\mu n}{a^2}\tilde{v}_n\right]\dfrac{\partial \tilde{w}_n^*}{\partial x} \end{array}\right\}, \tag{7}$$

which contain only the first derivatives. In this case, the energy flow can be estimated from the displacement components measured at two close cross-sections.

3. MEASUREMENT METHOD

3.1. WAVE-TYPE DECOMPOSITION

In order to determine the energy flow of a cylindrical shell, it is necessary to measure three orthogonl components of the displacement or acceleration in the midsurface of the shell. Practically, these components can be estimated from the measurements made on the outer surface of the shell using the following relationships [11]:

$$u_m = u - d\frac{\partial w}{\partial x}, \qquad v_m = \left(1 + \frac{d}{a}\right)v - \frac{d}{a}\frac{\partial w}{\partial \theta}, \qquad w_m = w, \tag{8}$$

where d is the distance between the main axis of the rotational accelerometer and the midsurface of the shell, and u_m, v_m and w_m are, respectively, the measured values in the axial, tangential and radial directions on the outer surface of the shell. To calculate the axial and tangential displacement components u and v, it is necessary to measure the radial displacement component w first.

Combining equations (3) and (8) gives

$$u_m = u_0 - d\frac{\partial w_0}{\partial x} + \sum_{n=1}^{\infty}\left(u_n - d\frac{\partial w_n}{\partial x}\right)\cos(n\theta + \theta_{n0}) = u_{m0} + \sum_{n=1}^{\infty} u_{mn}\cos(n\theta + \theta_{n0}),$$

$$v_m = v_0 + \sum_{n=1}^{\infty}\left[\left(1 + \frac{d}{a}\right)v_n + \frac{nd}{a}w_n\right]\sin(n\theta + \theta_{n0}) = v_0 + \sum_{n=1}^{\infty} v_{mn}\sin(n\theta + \theta_{n0}),$$

$$w_m = w_0 + \sum_{n=1}^{\infty} w_n\cos(n\theta + \theta_{n0}). \tag{9}$$

Note that u_{mn}, v_{mn} and w_n we are complex and they are characterized by an amplitude and phase (or real and imaginary parts). In order to determinate all the displacement components at frequencies below the cut-off frequency of the nth circumferential mode, it is required to perform the measurement of three orthogonal displacement components on at least $N = (2n - 1)$ positions (for a single-force excitation, $\theta_{n0} = n\theta_{10}$ holds, $\dot{N}$ will reduce to $n + 1$) at the cross-section of interest. The required minimum measurement position number depends on the number of unknown coefficients of the circumferential modes of interest. It is also noted that the separation distance between adjacent accelerometers should be less than $\pi a/n$ to satisfy the Nyquist spatial sampling criterion [14]. Since the calculation of u requires the first order derivative of w, the radial displacement component also needs to be measured at two adjacent cross-sections close to the cross-section of interest.

Although theoretically a vector containing N unknown quantities can be determined from N experimental data, the solution is usually unreliable because of measurement errors and ill-conditioned coefficient matrices due to inappropriate measurement locations selected. A reliable solution needs more than N measurement positions. The accuracy increases with increasing the number of measurement positions [10].

The method of least squares [10] can be used to determine u_{mn}, v_{mn} and w_n from the measured real and imaginary parts of u_m, v_m and w_m at more than $(2n - 1)$ position around a cross-section. For example, for the determination of the radial displacement component at frequencies below the $n = 3$ cut-off frequency, w_n can be obtained from the minimization of its error function

$$e_w = \sum_{i=1}^{N}\left[w_m^i - w_0 - \sum_{n=1}^{2} w_n\cos(n\theta + \theta_{n0})\right]^2, \tag{10}$$

where $N(> (2n - 1) = 5)$ is the total number of the measurement positions on the cross-section of interest and w_m^i is the measured radial displacement component at position i. To obtain a minimum value of the error function, both w_n and θ_{n0} need to be adjusted. The minimization of e_w is divided into two steps. The first step is to find optimal w_n (best fitting curve with the least error) for a given θ_{n0}. The second step is to determine the optimal θ_{n0} by finding the minimum value of the error $e_w(\theta_{n0})$. The final result of the two minimizations gives rise to the modal amplitude and true θ_{n0}.

3.2. METHOD OF TRANSFER FUNCTIONS

In equations (4), (5) and (7), the imaginary part of the product of two complex quantities can be determined from their cross-spectrum or their transfer functions with reference to the

same stable signal [3, 4]. For example,

$$\mathrm{Im}\{\tilde{u}_n^* \tilde{w}_n\} = \frac{2}{\omega^4}\,\mathrm{Im}\{G(a_{un}, a_{wn})\} = \frac{2}{\omega^4}\,\mathrm{Im}\{H^*(F, a_{un})\,H(F, a_{wn})\}\,G(F), \tag{11}$$

where F is reference signal, a_{un} and a_{wn} are the axial and radial acceleration components of the nth circumferential mode, $H(F, a_{un})$ represents the transfer function of a_{un} to F, $G(a_{un}, a_{wn})$ and $G(F)$ represent cross- and auto-spectra. Therefore, the energy flow in a cylindrical shell can be determined from the measured cross-spectra or transfer functions.

3.3. TRANSVERSE SENSITIVITY OF THE ACCELEROMETERS

The non-zero transverse sensitivity of an accelerometer indicates that the output of the accelerometer will not only be related to its main-axis acceleration but also to the transverse-axis accelerations. For a cylindrical shell, three orthogonal displacement components are present and coupled. The displacement component measured by an accelerometer is related to all three orthogonal displacement components at the accelerometer location. If $(u_\alpha, v_\alpha, w_\alpha)$ are the output from the three accelerometers with their main axes directed along the axial, tangential and radial directions, they can be related to the local outer surface displacement components (u_m, v_m, w_m) by

$$\begin{pmatrix} u_\alpha \\ v_\alpha \\ w_\alpha \end{pmatrix} = \begin{pmatrix} 1 & \alpha_{x\theta} & \alpha_{xr} \\ \alpha_{\theta x} & 1 & \alpha_{\theta r} \\ \alpha_{rx} & \alpha_{r\theta} & 1 \end{pmatrix} \begin{pmatrix} u_m \\ v_m \\ w_m \end{pmatrix}, \tag{12}$$

where $\alpha_{\alpha\theta}$ is the tangential component of the transverse sensitivity of the accelerometer whose main axis is directed along the axial direction. The transverse sensitivity components of each accelerometer can be determined experimentally [5]. Therefore, (u_m, v_m, w_m) can be determined at each location from the accelerometer outputs $(u_\alpha, v_\alpha, w_\alpha)$.

The transverse sensitivity is usually very small (less than 5%). If all three orthogonal displacement components are in the same order, the error caused by the accelerometer transverse sensitivity may be small and can be neglected. However, if one displacement component is much higher than the other components (for example, the axial vibration dominates at low frequencies for the breathing circumferential mode), equation (12) should be used to eliminate the contribution from other orthogonal displacement components when the small displacement component is measured.

3.4. JONG–VERHEIJ'S METHOD

Jong and Verheij [8] used the symmetrical nature of the circular cylindrical shell to decompose the circumferential modes at frequencies below the cut-off frequency of $n = 3$ circumferential mode, where the $n > 2$ circumferential modal displacement components are negligible. For example, the radial displacement component can be approximated as

$$w_m = w_0 + w_1 \cos(\theta + \theta_{10}) + w_2 \cos(2\theta + \theta_{20}), \tag{13}$$

where three modal amplitudes (w_0, w_1 and w_2) and two phase angles (θ_{10} and θ_{20}) have to be determined from the measurements. If eight measurement positions are uniformly localized around the shell surface at the cross-section of interest, as shown in Figure 2, the modal amplitudes and phase angles of the radial displacement component can be

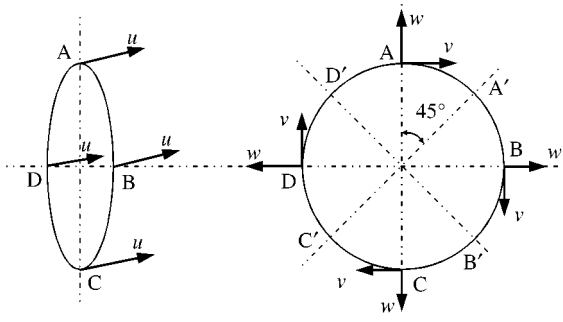

Figure 2. Accelerometer configurations for circumferential mode decomposition [8].

determined by the following equations:

$$w_0 = \frac{w_A + w_B + w_C + w_D}{4},$$

$$w_1 \cos\theta_{10} = (w_A - w_C)/2, \qquad w_1 \sin\theta_{10} = (w_D - w_B)/2,$$

$$w_2 \cos(\theta_{20}) = (w_A - w_B + w_C - w_D)/4,$$

$$w_2 \sin(\theta_{20}) = (w_{D'} - w_{C'} + w_{B'} - w_{A'})/4, \tag{14}$$

where w_A represents the radial displacement component measured at location A. In a similar way, the modal amplitudes and phase angles of the axial and tangential displacement components can also be determined.

4. EXPERIMENTAL RESULTS

4.1. EXPERIMENTAL SET-UP

As shown in Figure 1, a 2·2 m long steel circular cylindrical shell of $a = 32{\cdot}5$ mm and $h = 1{\cdot}7$ mm was used in the experiment. The shell was lying along the X direction of a Cartesian co-ordinate system. One end of the shell (0·5 m) was buried in a dry sand-filled box to provide an effectively absorptive termination for all circumferential modes and wavetypes. The other end of the shell was free and attached with a mechanical shaker which was driven with pseudo-random noise. A shaker was connected to an adaptor (angle of 45° to the X-axis and also to the plane of the end cross-section) which was attached to the inside wall surface of the shell. This arrangement allows the excitation of all the wave types in the shell. A piano wire fixed on a frame was used to provide a support at a position 0·5 m away from the free end.

The aim of this experiment is to demonstrate the feasibility of the above described measurement method. The circumferential modes of $n = 0$, 1, 2, 3 were considered and the frequency range of analysis was set upto 6 kHz (the cut-off frequencies of the $n =$ 2, 3, 4 circumferential modes are 1·03, 2·91 and 5·58 kHz, respectively, which are calculated by using the Love–Timoshenko theory [13]). Since the frequency characteristics of the shaker being used is not flat (decreases with increasing frequency after 1·36 kHz) in this frequency range, it is not possible to obtain a good signal-to-noise ratio using one input power level. Therefore, two sets of measurements were carried out. One is that the pseudo-random noise signal output from a signal generator was directly input to the shaker via a power amplifier and the upper frequency limit of the analyzer was set to 3·2 kHz. The

data at frequencies below the $n = 3$ cut-off frequency are obtained from this set of measurement. Another is to use an octave frequency filter which was set at the centre frequency of 4 kHz (the upper and lower frequency limits are 2825 and 5650 Hz) to ensure a good signal-to-noise ratio at frequencies between the cut-off frequencies of the $n = 3$, 4 circumferential modes.

To compare the power transmission with the input power, an impedance head was mounted at the driving location. The shaker and the impedance head were connected by a steel rod of 30 mm in length and 1 mm in diameter to avoid the transmission of possible transverse force which would cause errors in the input power measurement. The total input power can be calculated using the force and acceleration signals, F and a_s, output from the impedance head, that is

$$P_{input} = \frac{1}{2} \operatorname{Re} \{F^* v_s\} = \frac{1}{\omega} \operatorname{Im} \{G(F, a_s)\}, \tag{15}$$

which is referred to directly measured input power in the following sections. A B&K4375 accelerometer was used to pick up the radial acceleration signal. For the measurement of axial and tangential acceleration components, the same accelerometer was mounted on an aluminium cube of 10 mm side dimensions to construct a rotational accelerometer.

The transverse sensitivity of an accelerometer may depend on the frequency but the magnitude should be of the same order. Also, the axes where the accelerometer has its maximum and minimum transverse sensitivity readings should not be changed with frequency and they are orthogonal. To identify the maximum magnitude order and the minimum transverse sensitivity axis of the accelerometer, a B&K4294 Calibration Exciter and an aluminium cube were used. The maximum and minimum transverse sensitivity axes were marked on the accelerometer. The transverse sensitivity components in the two orthogonal transverse axes were 0·91 and 2·67%, respectively, at 159 Hz. During the measurements, the two orthogonal transverse axes (or the marked points) were directed along the axial, tangential or radial directions, respectively, depending on which acceleration component is of interest. The calculations using equation (12) and by assuming that the maximum and minimum transverse sensitivities are 5% ($> 2{\cdot}67\%$) and 1% ($> 0{\cdot}91\%$), respectively, indicate that for our experimental results the errors due to the presence of accelerometer transverse sensitivity are small ($< 1.8\%$) and negligible.

The cross-section of interest was 1·0 m away from the excitation end. In order to compare this proposed method with the method described in reference [8], two sets of measurement positions were chosen. For the measurements of the $n = 0$, 1, 2 tangential modal acceleration components, eight measurement positions were uniformly distributed (the radial angle between the neighbouring positions was 45°) around the cross-section, as shown in Figure 2. This set of measurement positions allows the comparison between the method proposed in this paper and the method presented by Jong and Verheij [8] based on the same data. Due to the increase of the circumferential modal number from 3 to 4 in the frequency range between the cut-off frequencies of $n = 3$ and 4, 16 measurement positions were chosen (the radial angle among the neighbouring positions was 22·5°) around the cross-section to increase the measurement accuracy. Every acceleration component (both real and imaginary parts) was recorded using the transfer function mode of an FFT analyzer with the force signal from the impedance head as the reference.

To minimize the positioning error of the transducer (the difference between the theoretically assumed transducer position and the actual measurement position), the measurement positions were marked before the measurements and care was taken during the measurements to ensure that the transducer was located at the marked points. The error

due to the positioning accuracy of the transducer depends on the property of the wavefield and the measurement location [15]. If the wavefield is not very reactive and the normalized positioning error (the ratio of the positioning error to the difference between the measurement (angular) positions) is less than 5% (or 10%), this type of error will be less than 3% (or 5%).

4.2. MEASUREMENT OF TRANSFER FUNCTIONS

The essence of this proposed method is to use the method of least squares to decompose the circumferential mode from the measured data. To assess its accuracy, the method proposed by Jong and Verheij [8] was used as a reference method in the frequency range below the cut-off frequency of $n = 3$ circumferential mode and the comparisons were made based on the same data. Equation (8) was used to eliminate the interaction between different wavetypes.

Figures 3–5 show the comparisons between the magnitudes of the acceleration components obtained using the methods of least squares and the method proposed in reference [8] respectively. It can be seen that the overall torsional response (tangential vibration component) is strong for all circumferential modes in the frequency range of interest. At frequencies below the cut-off frequency (1·03 kHz) of the $n = 2$ circumferential mode, the extensional mode (axial vibration component) has a larger response than the flexural mode for $n = 0$ while the flexural mode (radial vibration component) becomes larger for $n = 1$. The comparison of the two methods shows that a good agreement can be obtained when the circumferential modal response is relatively large. Difference in the measured responses occurs when the response is very small. The poor agreement appears especially in the frequency range above the cut-off frequency of the $n = 2$ circumferential mode. This could be partly due to the increase of circumferential mode number. For the same number of measurement positions, the accuracy of wave decomposition made by the method of least squares may decrease with increasing the number of unknown quantities [10].

Figure 6 shows the magnitudes of the $n = 3$ axial, tangential and radial acceleration components obtained using the methods of least squares at frequencies between the cut-off frequencies of the $n = 3, 4$ circumferential modes. All the magnitudes decrease with increasing frequency and become very small at frequencies close to the cut-off frequency of the $n = 4$ circumferential mode. The radial vibration level is the largest. The tangential vibration level is larger than the axial one at frequencies close to the $n = 3$ cut-off frequency but becomes smaller with increasing frequency. This figure also shows that the $n = 3$ cut-off frequency is 3016 Hz rather than 2·91 kHz predicted by using the Love–Timoshenko theory [13]. At frequencies below the $n = 3$ cut-off frequency and above the $n = 4$ cut-off frequency, the curves are not correct because the calculation is inaccurate.

4.3. MEASUREMENT OF ENERGY FLOW

The energy flow in a cylindrical shell can be calculated based on equations (4), (7) and (11) from the measured transfer functions. For the cylindrical shell being considered, the calculated wavenumbers indicate that only one propagating wave was present for each circumferential mode in the frequency range of interest and the decaying waves should become insignificant at frequencies above 5 Hz on the measurement positions. Therefore, equation (6) can be used. The first order derivatives of displacement or acceleration

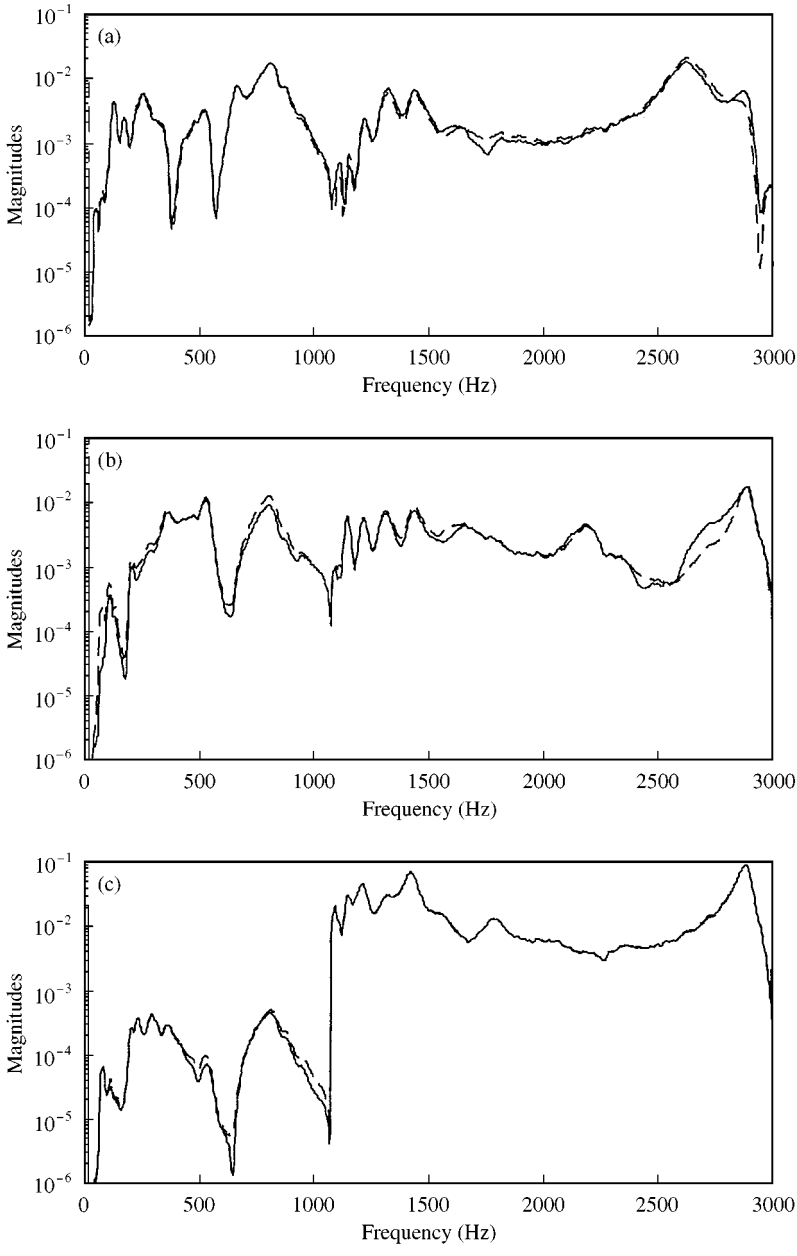

Figure 3. Measured magnitudes of the axial acceleration component for the circumferential modes of (a) $n = 0$, (b) $n = 1$ and (c) $n = 2$. respectively, by using the method of least squares (——) and the method proposed in reference [8] (– – – – –).

components were estimated from two measurements on the neighbouring cross-sections, the distance between which was 0·3 m ($n = 0$, 1, 2) or 0·12 m ($n = 3$) for extensional wavetype, 0·2 m ($n = 0$, 1, 2) or 0·08 m ($n = 3$) for torsional wavetypes and 15 mm ($n = 0$, 1, 2,) or 10 mm ($n = 3$) for flexural wavetype respectively. The finite difference error of each first derivative approximation was corrected using the following expression [16] during

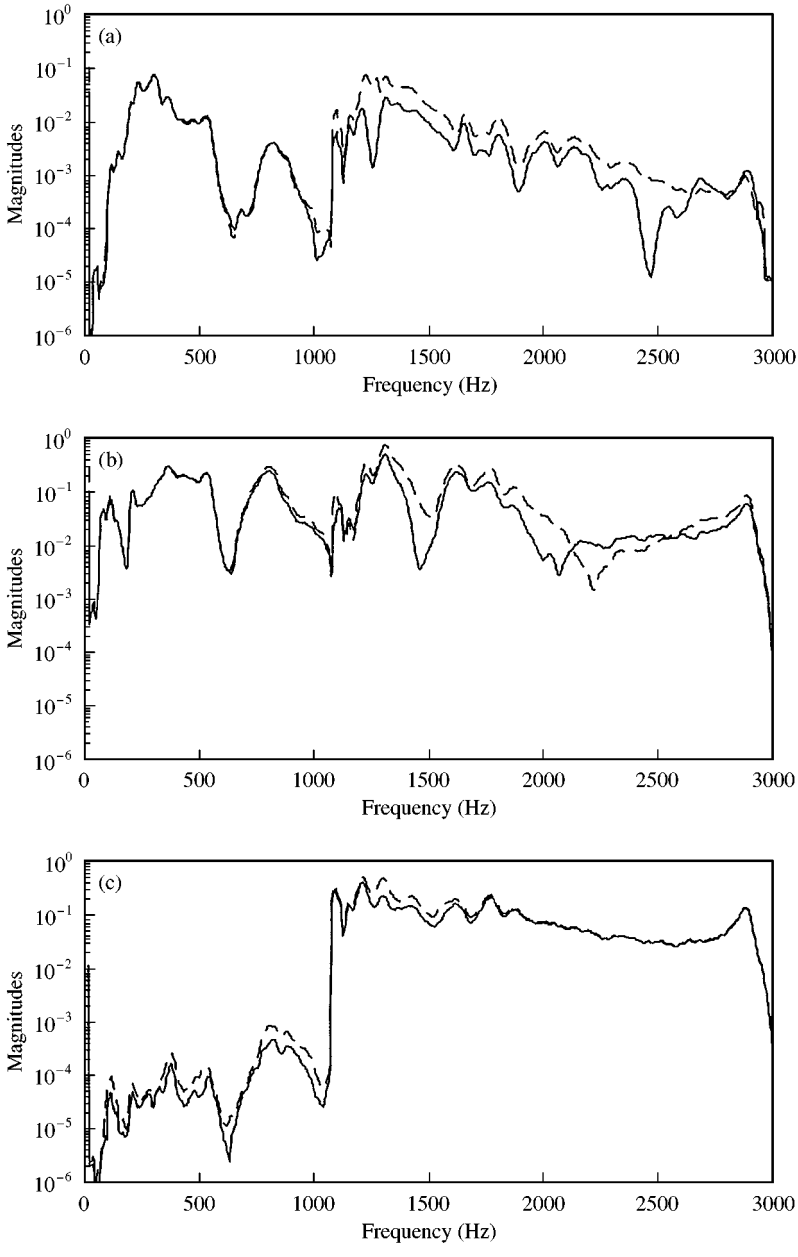

Figure 4. Measured magnitudes of the tangential acceleration component for the circumferential modes of (a) $n = 0$, (b) $n = 1$, and (c) $n = 2$, respectively, by using the method of least squares (——) and the method proposed in reference [8] (– – – – –).

data processing:

$$A_{corrected} = \frac{k\Delta}{\sin(k\Delta)} A_{measured}, \tag{16}$$

where $A_{measured}$ and $A_{corrected}$ represent the measured and corrected first order derivatives, Δ is the distance between the two measurement positions (or cross-sections) and k is the

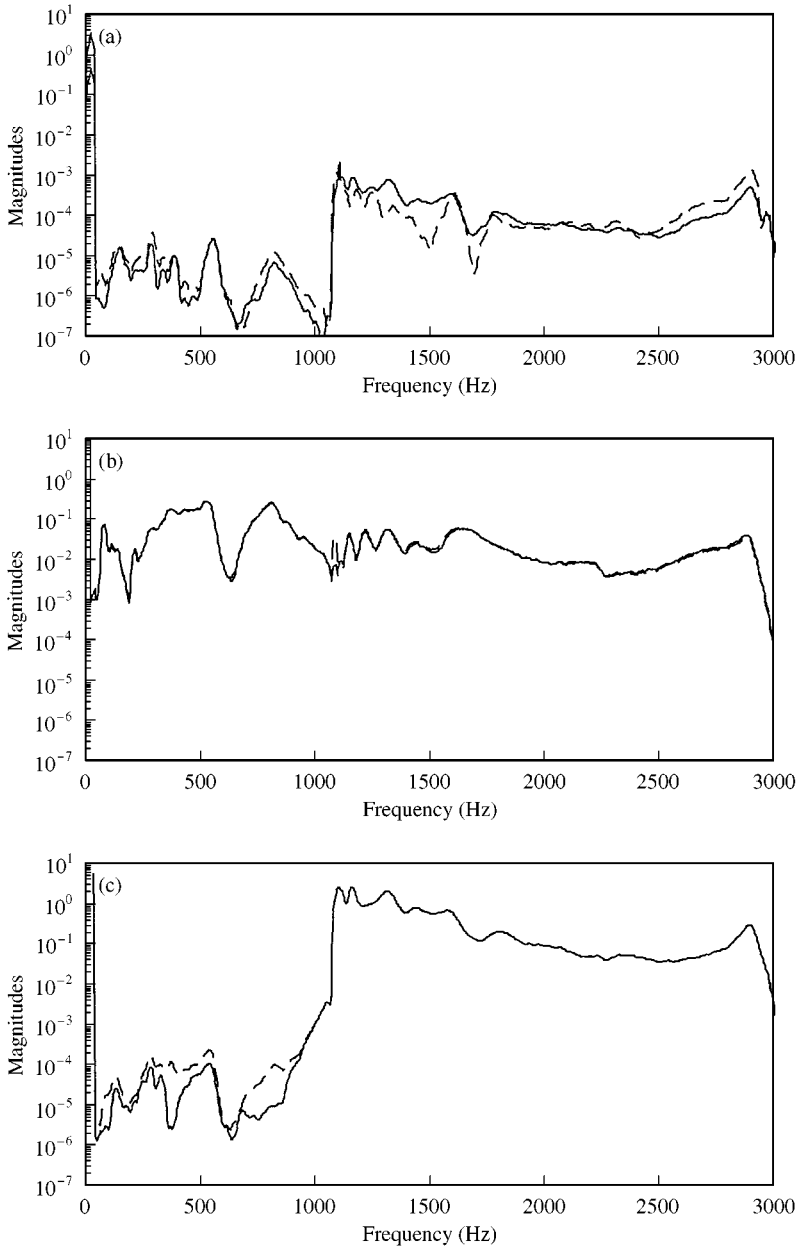

Figure 5. Measured magnitudes of the radial acceleration component for the circumferential modes of (a) $n = 0$, (b) $n = 1$ and (c) $n = 2$, respectively, by using the method of least squares (——) and the method proposed in reference [8] (– – – – –).

wavenumber. Figures 7(a) and 7(b) show the distance between wavelength ratios (Δ/λ) and the predicted normalized finite difference errors ($\varepsilon = (A_{corrected} - A_{measured})/A_{corrected}$) of extensional, torsional and flexural wave types. The jumps in the curves at 3 kHz result from the use of different distance values (Δ) below and above this frequency.

Figure 8 shows the comparisons of the energy flow components for the $n = 0, 1, 2$ circumferential modes obtained by the two methods respectively. The $n = 1$ energy flow

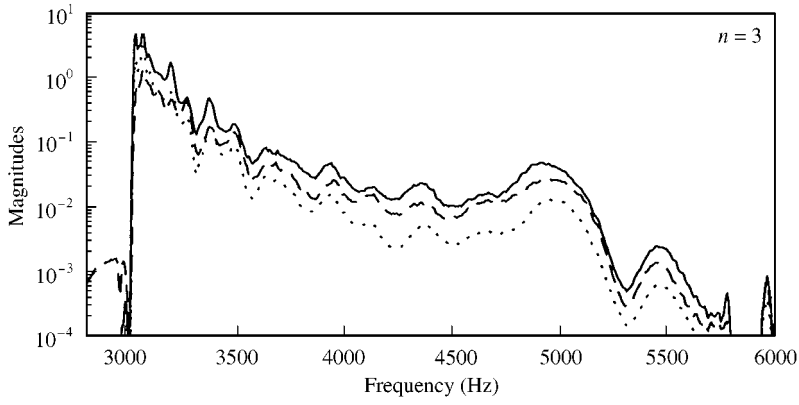

Figure 6. Measured magnitudes of the axial (– – – – –), tangential (- - - - -) and radial (——) acceleration components for the circumferential mode of $n = 3$ using the method of least squares (from 16 measurement positions).

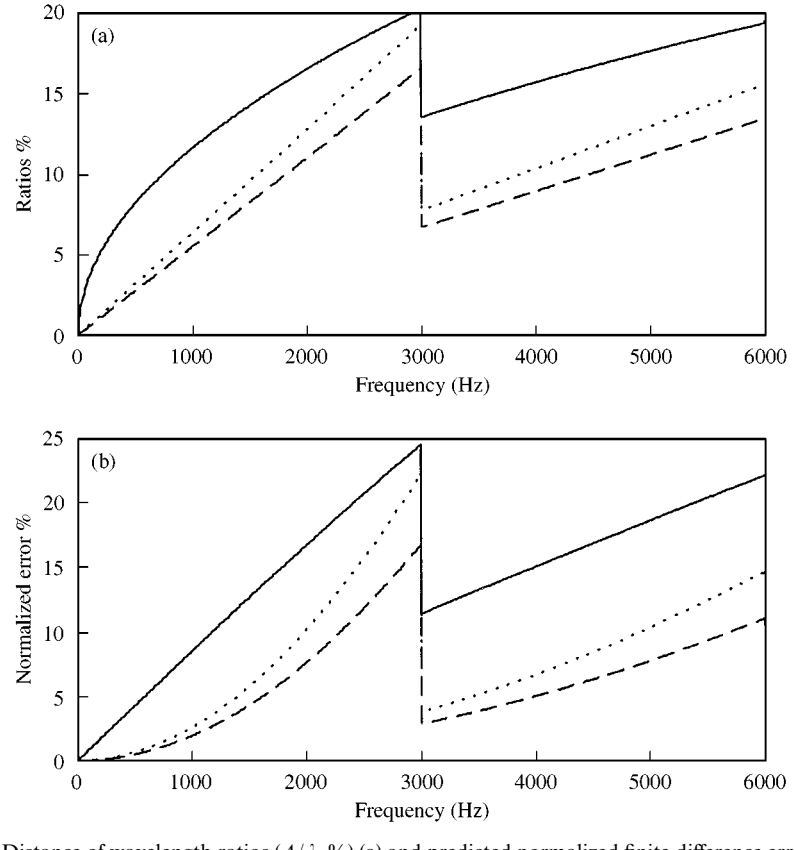

Figure 7. Distance of wavelength ratios (Δ/λ, %) (a) and predicted normalized finite difference errors (ε, %) (b) of the first order derivatives for extensional (– – – – –), torsional (- - - -) and flexural (——) wave types respectively.

component dominates at frequencies below the cut-off frequency of the $n = 2$ circumferential mode while the $n = 2$ energy flow component dominates at frequencies between the cut-off frequencies of the $n = 2$ and 3 circumferential modes. At very low frequencies (below 50 Hz for this measurement), the energy flow components seem

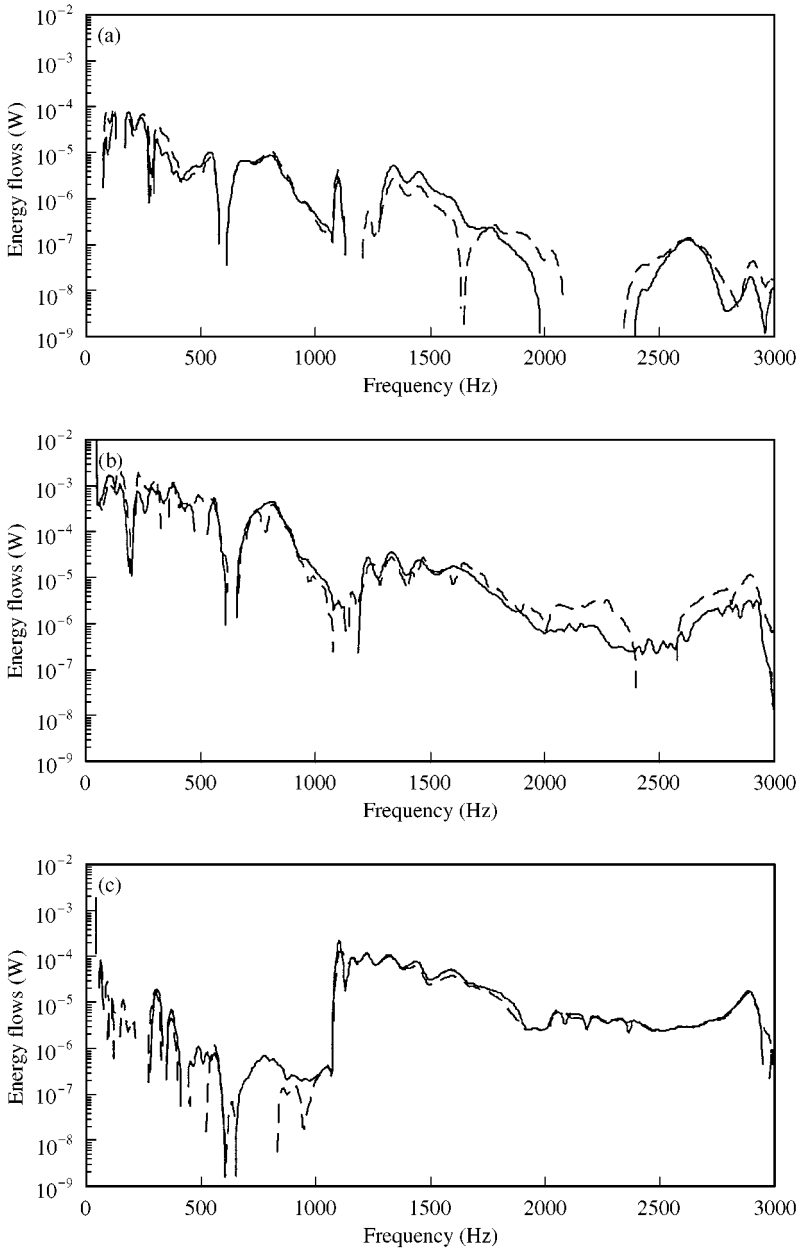

Figure 8. Measured energy flow components of the (a) $n = 0$, (b) $n = 1$ and (c) $n = 2$, circumferential modes, respectively, by using the proposed method (——) and the method described in reference [8] (– – – – –).

unmeasurable by either methods. The main reason could be due to a poor signal-to-noise ratio (Figures 3–5 show very small magnitudes for all the circumferential modes and all the wavetypes) and a very small energy flow resulting in a small phase change in the signals (for calculating the first derivative) measured on two neighbouring cross-sections. The measured signals were totally corrupted by noises. For the breathing mode $n = 0$, the agreement is good especially at low frequencies although some discrepancy is present but the curve

shapes are similar. The negative energy flow, which is not plotted in the figures, could be due to that the true energy flow was very small and the measured signals were corrupted by noises. For $n = 1$, the curves shapes are not similar at frequencies below 500 Hz but their values are close. For $n = 2$, the agreement is very good at frequencies above the cut-off frequency of the $n = 2$ circumferential mode. The disagreement at low frequencies is because no such energy flow was present and the measured data were residual.

Energy flow contains the information of magnitude and phase of displacement. The very good agreement in Figures 3–5 and some discrepancy in Figure 8 for the same circumferential mode indicate that a small phase difference is usually present between the results obtained by the two methods. There could be two possible reasons. The first is the positioning error of the transducer, that is, the actual measurement positions may slightly depart from the theoretically assumed positions. This could be the main error source for the method proposed in reference [8]. The second is that the method of least squares can only give approximate results, therefore, an error usually exists in each final result. This error should decrease with increasing the number of measurement positions.

Figure 9 shows the comparisons between the directly measured input power and the total energy flows obtained by the two methods. It can be seen that the total energy flows obtained by both methods agree well with the directly measured value. However, in the low (below 500 Hz) and high (above 2 kHz) frequency ranges the method proposed in this paper gives a better agreement with the direct measurement than the method presented in reference [8].

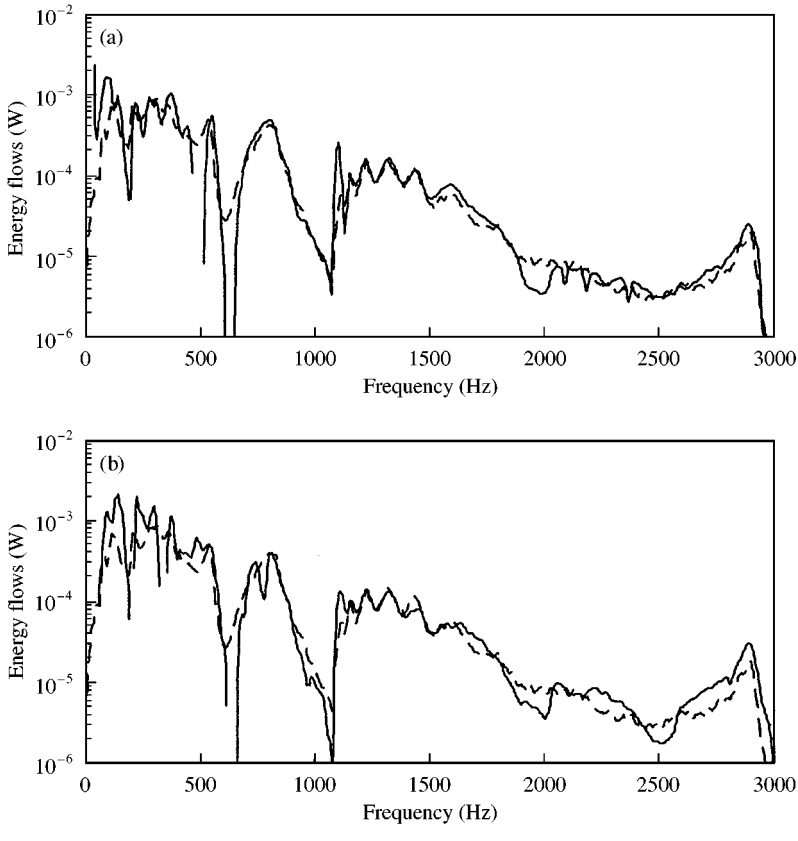

Figure 9. Comparisons between the directly measured input power (– – – –) and the total energy flows (——) measured by the proposed method (a) and the method described in reference [8] (b).

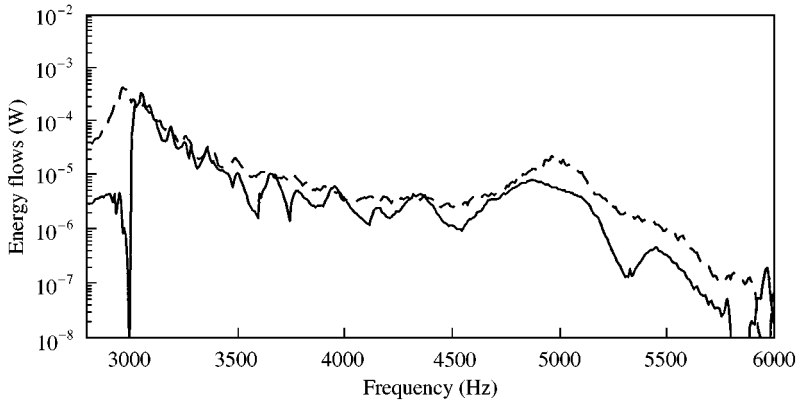

Figure 10. Comparisons between the directly measured input power (– – – –) and the total energy flow (——) measured using the proposed method (from 16 measurement positions).

Figure 10 shows the comparison between the directly measured input power and the total energy flow obtained by the proposed method at frequencies between the cut-off frequencies of the $n = 3$, 4 circumferential modes. The agreement is reasonably good especially at frequencies close to the $n = 3$ cut-off frequency. As frequency increases, the proposed method gives smaller values than the direct measurement. Possible reasons could be:

1. The input power decreased with increasing frequency resulting in a poorer signal-to-noise ratio at higher frequencies.
2. With increasing frequency the mass of the accelerometer may become significant compared with the modal mass of the shell. The effect of accelerometer mass loading was not considered during the data processing.

For a large diameter cylindrical shell, the cut-off frequencies of circumferential modes become smaller. The above errors could be reduced and the measurement accuracy of the energy flow carried by higher circumferential modes can be improved. The disagreement at frequencies below the $n = 3$ cut-off frequency is because the $n = 3$ circumferential mode was considered in this frequency range during the data processing.

5. CONCLUSIONS

A method is proposed in this paper to measure the energy flow through a thin-walled cross-section of a cylindrical shell. The outlines theory is experimentally verified on a steel cylindrical shell. The measured results demonstrate that in the frequency range below the cut-off frequency of the $n = 4$ circumferential mode, this new method can be used to accurately measure the total energy flow and its components. At frequencies below the $n = 3$ cut-off frequency, this method gives identical results as the existing method but it does not require that the cross-section of interest is fully accessed and that the measurement positions are uniformly distributed.

ACKNOWLEDGMENT

Support for this work from Australian Research Council is gratefully acknowledged.

REFERENCES

1. D. U. NOISEUX 1970 *Journal of the Acoustical Society of America* **47**, 238–247. Measurement of power transmission in uniform beams and plates.
2. G. PAVIC 1976 *Journal of Sound and Vibration* **49**, 221–230. Measurement of structure-borne wave intensity, Part I: formulation of the methods.
3. J. W. VERHEIJ 1980 *Journal of Sound and Vibration* **70**, 133–149. Cross spectral density methods for measuring structure borne power transmission on beams and plates.
4. J. LINJAMA and T. LAHTI 1992 *Journal of Sound and Vibration* **153**, 21–36. Estimation of bending wave intensity in beams using the frequency response techniques.
5. J. PAN, R. MING, C. H. HANSEN and R. L. CLARK 1998 *Journal of the Acoustical Society of America* **103**, 898–906. Experimental determination of the total vibratory power transmission in an elastic beam.
6. J. W. VERHEIJ 1986 *Multi-path sound transfer from resiliently mounted shipboard machinery*. Technisch Physische Dienst TNO-TH, Delft.
7. J. W. VERHEIJ 1990 *Noise Control Engineering Journal* **35**, 69–76. Measurements of structure-borne wave intensity on lightly damped pipes.
8. C. A. F. DE JONG and J. W. VERHEIJ 1992 *Proceedings of the 2nd International Congress on Recent Developments in Air and Structure-borne Sound and Vibration*, *March* 1992, *Auburn University*, *USA*, 577–585. Measurement of energy flow along pipes.
9. A. R. BRISCOE and R. J. PINNINGTON 1996 *Journal of Sound and Vibration* **192**, 771–791. Axisymmetric vibrational power measurement in empty and fluids filled pipes.
10. D. G. REES 1987 *Foundations of Statistics*. London: Chapman & Hall.
11. W. FLUGGE 1973 *Stresses in Shells*. Berlin: Springer-Verlag; second edition.
12. G. PAVIC 1990 *Journal of Sound and Vibration* **142**, 293–310. Vibration energy flow in elastic circular cylindrical shells.
13. A. W. LEISSA 1973 *NASA SP*-288, *Washington DC*. Vibration of shells.
14. C. R. FULLER, S. J. ELLIOTT and P. A. NELSON 1996 *Active Control of Vibration*. New York: Academic Press.
15. R. S. MING, J. PAN and M. P. NORTON 1999, *Technical Report*, *Department of Mechanical and Materials Engineering*, *The University of Western Australia*, *Nedlands*, *Australia*. Determination of the modal polarization angle of structural waves in a circular cylindrical shell.
16. J. W. VERHEIJ and C. J. M. VAN RUITE 1983 *Report* 308.785/1, *Institute of Applied Physics*, *TNO-TH*, *Delft*, *Holland*. On the measurement of structure-borne sound energy flow along pipes, Part 3: analysis of systematic and random errors.